Study of mercury adsorption by low-cost sorbents

using kinetic modeling

A. Fuente-Cuesta[ab], Ir. Diamantopoulou[c], M.A. Lopez-Anton[a*], M. Diaz-Somoano[a],

M.R. Martínez-Tarazona[a], G.P. Sakellaropoulos[c]

[a]Instituto Nacional del Carbón (CSIC). C/ Francisco Pintado Fe Nº 26, 33011, Oviedo, Spain

[b] Present address: School of Chemistry, University of St. Andrews, Fife KY16 9ST, United Kingdom

[c]Chemical Process Engineering Laboratory, Department of Chemical Engineering, Aristotle University of Thessaloniki, Thessaloniki, Greece

*Corresponding author

Phone: +34 985119090

Fax: +34 985297662

e-mail: marian@incar.csic.es

1

Abstract

In order to make further progress in the field of reducing mercury emissions to the atmosphere it is necessary to develop efficient and economically viable technologies. Low-cost solid sorbents are a candidate technology for mercury capture. However, kinetic models are required to predict the adsorption mechanism and to optimize the design of the process. In this study, several low-cost materials (biomass chars) were evaluated for the removal of gas-phase elemental mercury and kinetic studies were performed to investigate the mechanism of mercury adsorption. These kinetic studies were also used to predict the behavior of a fixed bed column. The models applied were pseudo-first and pseudo-second order equations, Fick´s intraparticle diffusion model and Yoon-Nelson´s model. The chars obtained from the gasification of plastic-paper waste demonstrated the best behaviour for mercury capture due to their high BET surface area, large total pore volume (mainly micropore volume) and high chlorine content. The Yoon-Nelson model provided a better fitting for the samples with low mercury retention capacities, while in the case of the plastic-paper chars all the models provided relatively accurate predictions because their highly microporous structure retarded the internal diffusion process and their increased chlorine content enhanced chemisorption on their surface.

Keywords: mercury; kinetic; char; biomass; combustion

1. Introduction

Mercury emissions to the atmosphere represent a huge threat to human health and methods to control them need to comply with a series of legislative regulations both in the European Union (EU) and worldwide.[1] To conform to these regulations, safe, clean and economically viable technologies must be employed.[2]

A large number of methods have been studied in order to solve the problem of mercury release. The conventional pollution abatement technologies have proven to be inefficient for controlling gas-phase mercury emissions and, in particular, the elemental form of mercury (Hg^0) [3] due to its high volatility and insolubility in water. Adsorption is the simplest and most efficient method for the removal of mercury. Activated carbon, a well known adsorbent, has been shown to have a good capacity for the capture both elemental and oxidized Hg. However, the high price that activated carbon can reach on the market, especially if it is impregnated with elements such as sulphur or choline, has encouraged efforts to find alternative adsorbents prepared from low-cost raw materials, such as agricultural residues, cheap biopolymers or waste tires,[4-6] and by-products from combustion plants, such as fly ashes.[7,8] In the present study mercury adsorption tests were performed using char samples obtained from the gasification of biomass (sunflower husks, poultry litter, wood and plastic-paper wastes). In previous studies,[9,10] some of these low-cost sorbents showed mercury retention capacities comparable to those of commercial activated carbons especially designed for the capture of Hg^0 in simulated coal combustion conditions.

The adsorption process itself needs to be studied, taking into account both equilibrium and kinetic criteria. This is because the performance of fixed bed columns depends not only on the capacity of adsorbents to adsorb pollutants but also on the rate of adsorption which is determined by adsorption kinetics.[11,12] Modelling the adsorption

of mercury on solids is important not only for purely theoretical reasons, but also for specific applications or for predicting the performance of commercial fixed bed reactors,[13,14] which finally will determine the design of the process. A number of kinetic models that describe heavy metal adsorption processes, mainly from liquid phase, have been studied.[15,16] Some of them are based on the diffusion of gas molecules inside the adsorbent porous network, while others take into account the pollutant mass balance inside the column. A very small number of studies have examined simplified models based on a combination of internal particle and external mass transfer theories with isothermal adsorption and powdered injection procedures.[17,18] In most of the kinetic studies reported in the literature, heavy metals adsorption from liquid phase by means of batch experiments have been modelled using pseudo-first and second order models and Elovich equations.[19,20] Apart from the above kinetic models that describe the adsorption of mercury ions from liquid phase, there is a small amount of information available in the literature on the adsorption kinetics of gas phase mercury on adsorbents.[13,21] The main problem arises from applying kinetic equations without having first closely analyzed the mercury adsorption mechanism involved and without having taken into account their disadvantages. These are the issues that will be addressed in the present work.

This study attempts to improve the current level of understanding of the adsorption of elemental mercury by applying four simplified kinetic models, i.e. intraparticle-diffusion, pseudo-first and pseudo-second order equations and a mass balance in the fixed bed reactor. The kinetics study was carried out with chars obtained from the gasification of biomass that have until now received very little attention but are considered to be good candidates for mercury capture.
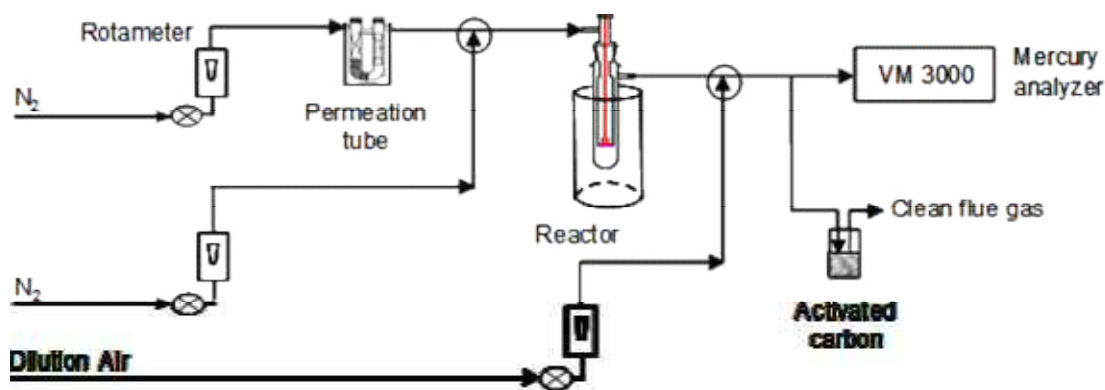
2. Experimental

2.1. Material selection and characterization

The five biomass gasification chars used in the study were produced at the Energy Research Centre of the Netherlands (ECN) in a 500 kW pilot plant equipped with a circulated fluidized bed gasifier (BIVKIN). The samples were designated as follows: SH refers to the gasification char from the sunflower seed shells, PL to the char from chicken manure, WW1 to the char derived from wood wastes, and both PW1 and PW3 to the chars obtained from the plastic-paper wastes. The only difference between the procedure for obtaining PW1 and PW3 was the gasification temperature employed.

A full physico-chemical characterization of these biomass gasification chars can be found elsewhere.[9] The pore size distribution of the samples was determined by applying the quenched solid Density Functional Theory (QSDFT) method for the N_2 adsorption isotherms, together with a slit-shape model to describe the micropore shape, and non-local DFT (NLDFT) for the CO_2 adsorption isotherms.[22,23] These methods were implemented using Quantachrome´s data reduction software. The particle size analysis was performed on a Beckman Coulter LS 13320 device, over a range of 0.04-2000 μm.

2.2. Mercury adsorption experiments

The experimental device employed for the mercury retention experiments at laboratory scale using the chars obtained from the biomass materials has been described in detail elsewhere[9] (Figure 1).

Figure 1. Schematic diagram of the lab-scale experimental device for mercury retention.

Most of the adsorption tests were carried out using 20 mg of char mass, mixed with 60 mg of sand, in a differential-bed reactor equipped with a glass column of inner diameter 0.3 inches enclosed in a temperature-controlled oven. The experiments were performed at 150ºC at a N_2 flow rate of 0.5 L min^{-1}. Depending on the final application of the sorbents, other gases such as O_2, SO_2, NOx, may be present with the mercury and have an effect on the adsorption capacity.[9,10] However, in this work the retention experiments were carried out in a nitrogen atmosphere to prevent the mercury from oxidising and to facilitate the kinetic study of the adsorption of elemental mercury. The mercury concentration in gas phase was 110±9 µg m^{-3}. The mercury capture experiments were carried out until the samples reached their maximum adsorption capacity.

3. Results and discussion

3.1. Adsorbent characterization

The most important conclusions drawn from the characterization of the samples studied have already been discussed in a previous work.[9] However the most interesting

results that may help to interpret the findings of the present work are shown in Table 1. The chars examined have a high mineral content ranging from 45% to 75% of ashes with only char SH showing a lower content, approx. 22% (Table 1). It is this wide range of mineral content that motivated this investigation of their ability to retain elemental mercury, since it is their high inorganic content that probably catalyzes the oxidation/adsorption of elemental mercury.[10] All of the samples have a low apparent surface area compared to that of conventional activated carbons, with the samples obtained from plastic-paper wastes presenting the largest specific surface area, total pore volume and micropore volume (Table 1). It should also be noted that their QSDFT and NLDFT pore size distribution curves are of a similar shape and reveal a narrow pore size distribution, with most of their total pore volume corresponding to pore widths of less than 4 nm. The particle sizes range from approximately 30 to 60 μm. Although it is generally assumed that oxygen functional groups play an important role in mercury capture, a previous study carried out by the authors using the same chars[9] showed that there was no relation between mercury retention and surface oxygen groups.

Table 1 – Ash and chlorine content, surface area, total pore volume and micropore volume by DR to the N_2 adsorption, and experimental mercury adsorption capacities obtained from an analysis of the spent adsorbent.

Sample	Ash content (%)	Cl (%)	BET surface ($m^2\,g^{-1}$)	V_{tot} ($cm^3\,g^{-1}$)	V_{mN2} ($cm^3\,g^{-1}$)	Hg adsorption capacity ($\mu g \cdot g^{-1}$)
SH	21.7	0.76	5	0.006	0.002	<1
PL	74.9	1.79	12	0.013	0.005	1.1
WW1	45.4	3.0	2	0.005	0.001	2.7
PW1	45.1	4.65	65	0.045	0.030	135
PW3	75.4	5.92	20	0.021	0.009	65

3.2. Mercury adsorption results

The mercury breakthrough curves for the examined adsorbents are presented in Figure 2, while the mercury contents of the spent adsorbents, determined by means of an automatic mercury analyzer AMA, together with some physical and chemical characteristics of the chars are shown in Table 1.
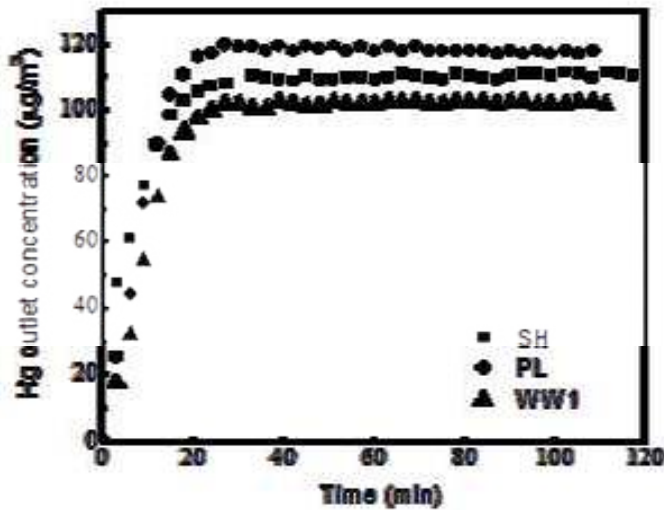
(A)
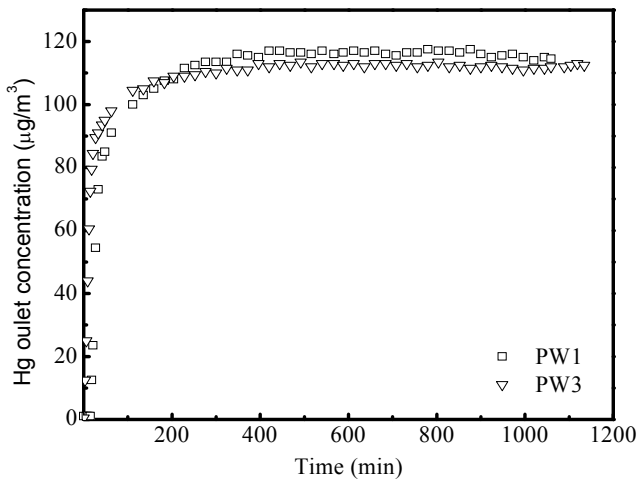
(B)

Figure 2. Hg^0 breakthrough curves (a) Sunflower husks, poultry litter and waste wood chars (b) plastic-paper chars.

The mercury adsorptive capacity of the adsorbents obtained from plastic-paper materials ranges between 65 and 135 µg/g, which is much higher than the values reached by the SH, PL and WW chars (Table 1). This can be attributed to the larger BET surface areas and total pore volumes of plastic-paper chars, although almost all of the examined materials have a microporous structure.[9] The greater mercury adsorption capacity of the plastic-paper chars may be due to the availability of chemisorption sites on their surface, where chlorine atoms cause the oxidation of elemental mercury. In many studies it has been established that the adsorption energy of elemental mercury on the surface of adsorbents with halogen is much greater than when no halogen is present. This indicates that impregnation with halogen increases the activity of neighbouring sites, thereby enhancing the capacity of the adsorbent surface to adsorb mercury.[24]

3.3. Adsorption kinetics

3.3.1. Langmuir adsorption models

3.3.1.1. Theoretical approach

The Langmuir isotherm assumes an idealized type of adsorption in that (i) the gas phase molecules are adsorbed at discrete points of attachment on the surface, (ii) the energy of the adsorbed species is the same everywhere on the surface and (iii) monolayer adsorption occurs because of physisorption by the micropores or/and chemisorption on the active sites. The curves of any adsorbed amount q versus time t, can be plotted by means of Equation 1.

$$q = q_t = \frac{F}{m} \cdot (C_{in} - C_{out}) \cdot t \qquad (1)$$

where q is the adsorbed amount of mercury at various times (µg/g), C_{in} is the initial mercury concentration (µg / m^3), C_{out} is the mercury concentration at the reactor outlet (µg / m^3), F is the volumetric gas flow (m^3 / min), m is the adsorbent mass (g) and t is the adsorption time (min).

The kinetic approach for deriving a mathematical expression from the Langmuir isotherm, where desorption is ignored, assumes that the rate of adsorption on the surface is proportional to the product of the gas phase concentration and the fraction of the vacant surface sites 1-θ:

$$\frac{d\theta}{dt} = k_a \cdot c \cdot (1 - \theta) \qquad (2)$$

Substituting q/q_e for the term θ, the above equation is transformed to:

$$\frac{dq}{dt} = k_a \cdot c \cdot (q_e - q) \qquad (3)$$

In Equation 3, for a constant gas phase concentration c, the term $k_a \cdot c$ can be replaced by the kinetic constant k_1, resulting in the pseudo-first order equation:[25,26]

$$\frac{dq}{dt} = k_1 \cdot (q_e - q) \Rightarrow q = q_e \cdot [1 - \exp(-k_1 \cdot t)] \qquad (4)$$

where q_e is the equilibrium adsorbed amount (µg / g) and k_1 is the kinetic constant in a pseudo-first order model (min^{-1}).

As can be seen from the pseudo-first order kinetic model, the rate of gas phase removal is proportional to the first order of available concentration of active sites on the adsorbent´s surface.

However, there is evidence to suggest that certain chemical adsorption processes involve the dissociation of the adsorbate to form two bonds with the adsorbent surface. In this case the kinetic approach to the derivation of the Langmuir equation requires that the process be regarded as a reaction between the gas molecule and two surface sites. In the case of strong adsorption, where the role of desorption is ignored, the reaction is expressed by means of the following equation:[27]

$$\frac{d\theta}{dt} = k_a \cdot c \cdot (1 - \theta)^2 \qquad (5)$$

By replacing the term θ with q/q_e, Equation 5 is transformed to:

$$\frac{dq}{dt} = \frac{k_a \cdot c}{q_e} \cdot (q_e - q)^2 \qquad (6)$$

In the above formula, the term $(k_a \cdot c)/q_e$ is replaced by the kinetic constant k_2 resulting in a pseudo-second order equation, in which the rate of adsorption is proportional to the second order of the concentration of available active sites on the adsorbent´s surface:

$$\frac{dq}{dt} = k_2 \cdot (q_e - q)^2 \Rightarrow q = \frac{t}{\left(\frac{1}{k_2 \cdot q_e^2}\right) + \left(\frac{t}{q_e}\right)} \qquad (7)$$

where k_2 is the kinetic constant in the pseudo-second order model (g/μg · min).

According to many studies, the pseudo-second order kinetic model represents the liquid phase chemisorption of divalent metals, such as ionic mercury Hg^{2+} on solid surfaces that occurs through an electron transfer process.[28,29] In the present study, the experimental results indicate that mercury retention occurs on char samples at high adsorption temperatures, where physisorption was limited. Thus, the kinetic approach to the derivation of the Langmuir equation seems to give promising results.

3.3.1.2. Results of fitting – Discussion

The evolution of the amount of adsorbed mercury with time for each sample, based on the mercury breakthrough curves, was calculated from Equation 1. The parameters k_1, k_2 and q_e were estimated by fitting the experimental data to the postulated model either via the pseudo-first order (Eq. 4) or the pseudo-second order (Eq. 7) kinetic model using non-linear regression methods. The fitting was performed for the period of time during which the curves show an exponential trend up to the point where equilibrium has been reached, when the mercury outlet concentration is close to 90-95 % of the inlet concentration.

The best fitting results are achieved by minimizing the deviation between the experimental and theoretical curves of Hg^0 uptake at various times, as a percentage of the maximum predicted value q:[30,31]

$$DEV(\%) = \frac{\sqrt{OF/(Z-M)}}{\max(q_{exp})}$$ (8)

where DEV(%) is the percentage of deviation, OF is the objective function, Z is the number of measured data points, M is the number of model parameters and max (q_{exp}) is the maximum experimental mercury uptake.

The optimization procedure requires that the objective function (OF), which is the square of the difference between the experimental vector values and the calculated ones, be minimized:

$$OF = \sum_{1}^{n} (q_{exp} - q_{pred})^2$$ (9)

where q_{exp} (µg/g) is the experimental Hg^0 uptake and q_{pred} (µg/g) is the predicted Hg^0 uptake.

Moreover, the percentage of the deviation between the experimental and theoretical breakthrough curves predicted by the models (C_{out} vs t) derived from Eq. 1 were calculated by the same procedure as that described above for the curves q vs t.

The fitted breakthrough curves of the pseudo-first and pseudo-second order kinetic models, along with the experimental data, are shown in Figure 3 for the SH and PW1 chars, these being representative examples of samples with low and high mercury retention capacities, respectively. The calculated parameters k_1,q_e and k_2,q_e for all the samples, as well as the percentages of deviation between the experimental and theoretical uptake and breakthrough curves, are presented in Table 2 (a) for the pseudo-first and (b) for the pseudo-second order models, respectively.
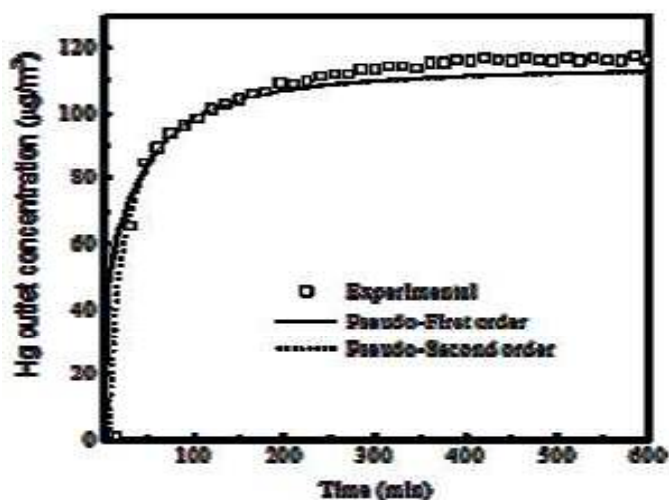
(A)
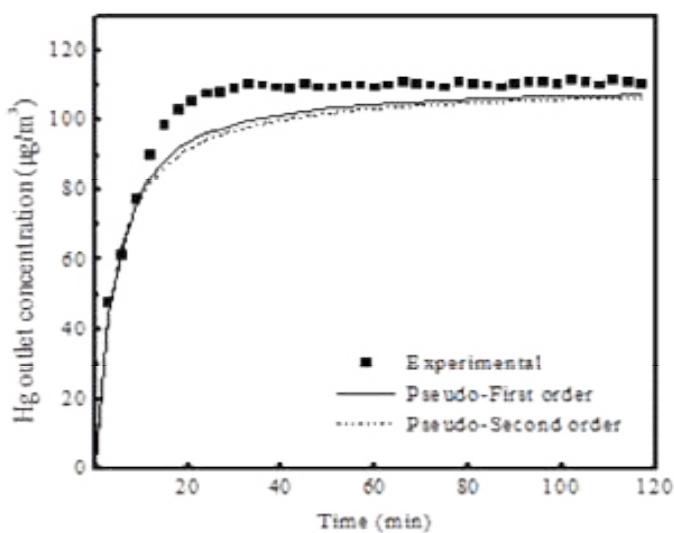
(B)

Figure 3. Experimental and calculated Hg^0 breakthrough curves for the (a) SH and (b) PW1 chars obtained by means of pseudo-first and pseudo-second order models.

In Figure 3 it can be seen that there is good agreement between the experimental data and the theoretical curves derived from the pseudo-first and pseudo-second order models, especially in the case of the PW chars (the samples with a high mercury capacity). Moreover, the predictions of the two models are very close. In almost all the cases the percentage of deviation is less than, or close to, 10% for the q vs t and C$_{out}$ vs t

curves. The best adjustments correspond to the PW chars, where almost all the deviations are less than 5%. This could be due to the larger number of experimental data collected for this group of samples as a result of the slower adsorption. The successful fitting of the adsorption procedure achieved using the kinetic models derived from Langmuir theory indicates that chemisorption on one or two active sites is the predominant mechanism of total adsorption for these adsorbents. The chemisorption mechanism might involve the oxidation of elemental mercury to Hg^{+1} or Hg^{+2} on the adsorbent´s surface through the carbon-oxygen group active sites or due to an increase in the chlorine content, especially in the case of the PW chars.[9,10] This possibility is reinforced by the high adsorption temperature employed in this study (150ºC), when physisorption can be expected to be limited. The kinetic constants predicted by both models for the PW chars are one order of magnitude smaller than for the other chars, indicating that the adsorption process is much slower in these samples. It should also be noted that the theoretical equilibrium adsorption capacity, q_e, predicted by both models, is higher than the experimental values obtained for samples SH, PL and WW1, whereas it is smaller in the case of the PW chars (Tables 1 and 2).

Table 2 - Kinetic data obtained by using (a) pseudo-first and (b) pseudo-second order models for mercury adsorption on biomass gasification chars.

(A)

Sample	R^2	Predicted Hg adsorption capacity $q_{e(pred)}$ ($\mu g/g$)	Deviation q vs t (DEV%)	Deviation C_{out} vs t (DEV%)	Kinetic constant k_1 (min^{-1})
SH	0.991	8.30	5.41	4.29	0.305
PL	0.982	11.6	7.63	8.90	0.343
WW1	0.988	12.2	6.19	9.98	0.270
PW1	0.957	44.0	4.09	6.83	0.042
PW3	0.926	24.4	4.82	4.41	0.040

(B)

Sample	R^2	Predicted Hg adsorption capacity $q_{e(pred)}$ ($\mu g/g$)	Deviation q vs t (DEV%)	Deviation C_{out} vs t (DEV%)	Kinetic constant k_2 ($g/\mu g \cdot min$)	Initial adsorption rate $1/k_2.qe^2$ ($g \cdot min /\mu g$)
SH	0.987	10.9	6.59	5.22	0.0257	0.3275
PL	0.975	14.8	8.89	10.3	0.0229	0.1994
WW1	0.984	16.7	7.24	12.3	0.0138	0.2598
PW1	0.964	48.1	3.77	4.64	0.0017	0.2542
PW3	0.948	29.9	6.09	3.83	0.0015	0.7457

3.3.2. Internal Diffusion Model

3.3.2.1. Theoretical approach

This model assumes that the mercury adsorption capacity of the adsorbents is controlled by an internal diffusion process. The particle mass balance yields the adsorption rate equation for the reactant component, which can be expressed in the generalized form:

15

$$\frac{\partial q}{\partial t} = D_{eff} \cdot \left(\frac{\partial^2 q}{\partial r^2} + \frac{2}{r} \frac{\partial q}{\partial r} \right) \tag{10}$$

where q is the adsorbed amount of mercury (µg / g), r is the radial distance (cm) and D_{eff} is the effective diffusivity coefficient (cm^2 / min).

Fick´s diffusion equation (Equation 10) is applied for initial conditions $q(r,0)=q_0$ and $\left(\frac{\partial q}{\partial r} \right)_{r=0} = 0$, it being assumed that effective diffusivity is constant and the amount adsorbed is calculated by means of Equation 1.

Equation 10 correlates the rate of mercury adsorption to particle diffusion by calculating the amount of mercury adsorbed per gram of adsorbent, q. It is applied in this study because most of the examined adsorbents have a microporous structure. Given that there is a strong interaction between the substance and the adsorbent surface, the diffused molecules cannot escape from the potential field of the adsorbent surface and they jump between adjacent sites. In light of the above analysis, the contribution of surface diffusion to mercury mass transfer inside the pores of the adsorbents can be expected. Therefore, the effective diffusivity coefficient employed is a function of the Knudsen and surface diffusion coefficients, D_K and D_S respectively.[32]

To solve Equation 10, the method of separation of variables has been adopted.[33]

$$\frac{q - q_1}{q_0' - q_1} = 1 + \frac{2R_p}{\pi \cdot r} \sum_{n=1}^{\infty} \frac{(-1)^n}{n} \sin \frac{n \cdot \pi \cdot r}{R_p} \exp\left(-D_{eff} \cdot n^2 \cdot \pi^2 \cdot t / R_p^2 \right) \tag{11}$$

where q_1 is the initial solid state concentration for a spherical particle (µg / g) and q_0' is the constant solid state concentration for a spherical particle (µg / g).

Thus, the total amount of diffusing substance entering the sphere is represented by:[32,33]

$$\frac{q}{q_e} = 1 - \frac{6}{\pi^2} \sum_{n=1}^{\infty} \frac{1}{n^2} \exp\left(-\frac{n^2 \cdot \pi^2 \cdot D_{eff} \cdot t}{R_p^2} \right) \tag{12}$$

where t is the experimental adsorption time, q/q_e is the equilibrium capacity calculated from the experimental breakthrough curves, D_{eff} is the effective diffusivity coefficient and Rp is the adsorbent particle radius (29, 38, 55, 58 and 57 μm for SH, PL, WW1, PW1 and PW3, respectively).

In the above equation, the diffusion time constant π^2*D_{eff}/R_p^2, which expresses a global kinetic constant, and the equilibrium capacity q_e, were calculated using a fitting procedure. The optimization procedure involves a non-linear algebraic model fitting problem, which is solved by a methodology described in a previous work, and as well as in other model fitting studies.[33,34]

3.3.2.2. Results of fitting – Discussion

The data for the quantities of mercury adsorbed with time were fitted to Eq. (12). Based on the results of q versus t predicted by this model, the theoretical breakthrough curves were obtained by means of Eq. (1). The predicted and experimental breakthrough curves, for the SH and PW1 chars are shown in Figure 4. The calculated parameters q_e and $\pi*D_{eff}/R_p^2$, as well as the percentages of deviation between the experimental and the theoretical uptake and breakthrough curves, are presented in Table 3.

(A)

17
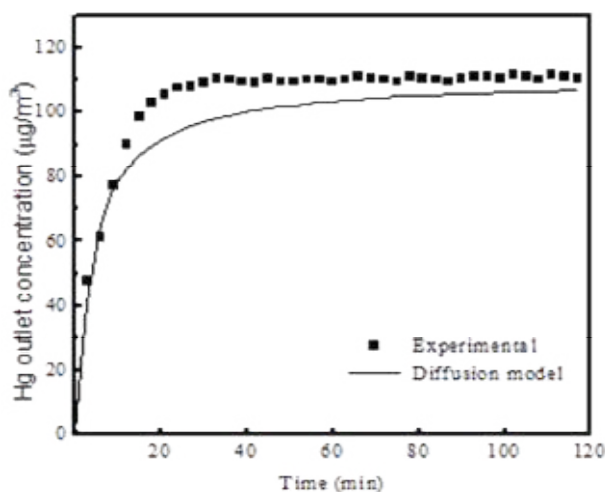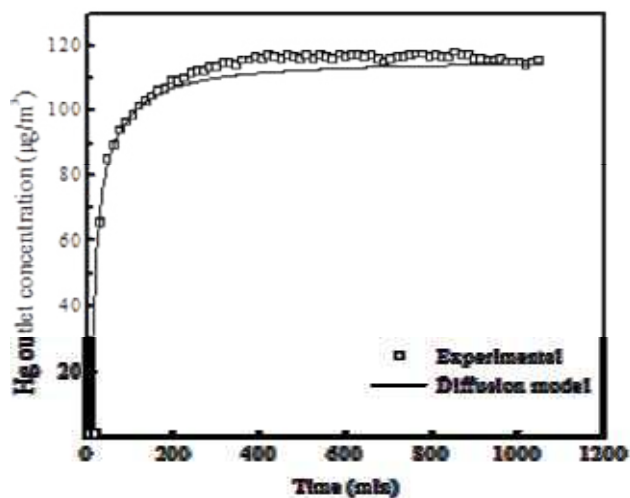
(B)

Figure 4. Experimental and calculated Hg^0 breakthrough curves for the (a) SH and (b) PW1 chars obtained by means of the Diffusion model.

Fick's diffusion model estimates relatively well the rate of mercury adsorption, especially for the PW chars, since the percentage of deviation varies between 4-5% in the case of the q vs t curves, and between 2-5% in the case of the C_{out} vs t curves (Figure 4 and Table 3). This indicates that the diffusion process inside the pore network of the adsorbents is taking place while adsorption is occurring on their active sites and both phenomena must be taken into account in order to describe the total mechanism of gas phase mercury uptake. However, for SH, PL and WW1 a better fit is achieved with the pseudo-first order model, since the deviation in the case of the q vs t curves ranges from 5 to 8% approx., whereas with the pseudo-second order model it ranges from 7 to 9% and with the diffusion model from 8 to 11%. Since the SH, PL and WW1 chars exhibit a fast column breakthrough and short adsorption times, the above results are in accordance with the observation that the pseudo-first order equation accurately predicts the initial period of adsorption.[26,28,35]

18

Table 3 - Kinetic data obtained by the diffusion model for mercury adsorption on biomass gasification chars.

Sample	Predicted Hg adsorption capacity $q_{e(pred)}$ (μg/g)	Deviation q vs t (DEV%)	Deviation C_{out} vs t (DEV%)	Kinetic constant $K_{diffus.}$ ($\pi^2 * D_{eff}/R_p^2$) (min^{-1})
SH	10.0	7.88	5.12	0.01103
PL	11.3	10.6	8.73	0.02767
WW1	13.4	9.52	10.9	0.01322
PW1	44.8	3.59	5.39	0.00283
PW3	25.3	5.52	2.11	0.00246

The adsorption capacities, $q_{e(pred)}$, predicted with this model, as well as the ones predicted with the models derived from Langmuir´s theory, differ from the experimental retention capacities (Tables 1 and 3). These differences in the case of samples SH, PL and WW1 can be attributed to their low retention capacities that make a good theoretical prediction difficult to achieve, whereas for the PW chars a good prediction requires a model which takes into account both stages simultaneously.

3.3.3. Fixed bed mass balance- Yoon and Nelson Model

3.3.3.1. Theoretical approach

The above models are based on complicated equations that describe surface diffusion in adsorbent particles and mercury adsorption on adsorbent active sites. Differential mass balance equations for an element in the adsorption column and for an adsorbent particle within such an element provide a good basis for developing a mathematical model able to describe the dynamic behavior of the system. If the flow pattern is represented as an

axially dispersed plug flow, the differential fluid mass balance is represented by Equation 13:[32]

$$\frac{\partial C_b}{\partial t} + u \cdot \frac{\partial C_b}{\partial z} + \left(\frac{1-\varepsilon}{\varepsilon}\right) \cdot \frac{\partial \overline{q}}{\partial t} = D_{ax} \cdot \frac{\partial^2 C_b}{\partial z^2} \qquad (13)$$

where C_b is the bulk phase concentration of mercury inside the column ($\mu g/m^3$), u is the superficial velocity of mercury in the column (cm/min), ε is the bed porosity, z is the axial direction in the column (cm) and $\overline{q}$ is the mean adsorbed quantity in the adsorbent particle ($\mu g/g$).

In an ideal plug flow system with no resistance to mass transfer, by neglecting the axial dispersion term and by assuming that the rate of adsorption is given by a first order kinetic expression k · c, Equation 13 can be simplified to Equation 14:[36]

$$-u \cdot \frac{\partial C_b}{\partial z} = k \cdot C_b \qquad (14)$$

In Equation 14 the constant k is replaced by the following expression proposed by the literature:[36]

$$k = k_0 \cdot \left[\frac{1}{1 + h_0 \cdot \frac{q}{q_e}} - \frac{\frac{q}{q_e}}{1 + h_0} \right] \qquad (15)$$

where k is the kinetic constant, k_0 is the initial value of k and h_0 is the dimensionless variable.

According to the Adams – Bohart model, the term q / q_e included in Equation 15, is related to the time t and axial distance z through the following expression:[36,37]

$$\frac{q}{q_e} = \frac{1 - \exp\left(\frac{k \cdot L}{u} \cdot \frac{t}{t_s}\right)}{1 + \exp\left(-\frac{k \cdot L}{u} \cdot \frac{t}{t_s}\right)\left[\exp\left(\frac{k \cdot z}{u}\right) - 1\right]} \qquad (16)$$

where L is the length of the column (cm) and t_s is the saturation time (min).

Thus, Equation 14 is solved by employing Equations 15 and 16, from which the following simplified Yoon-Nelson model is derived:[38,39]

$$t = \frac{q_e \cdot m}{C_{in} \cdot F} - \frac{q_e \cdot m}{C_{in} \cdot F \cdot k} \cdot \ln\left(\frac{C_{in} - C_{out}}{C_{out}}\right) \qquad (17)$$

where C_{in} is the mercury column inlet concentration ($\mu g/m^3$), C_{out} is the mercury column outlet concentration ($\mu g/m^3$), m is the mass of adsorbent (g) and F is the volumetric gas flow (m^3/min).

Equation 17 describes the solution for the breakthrough curve obtained from the differential fluid phase mass balance. By replacing the term $(q_e m)/(C_{in} F)$ with the time required for 50 % of breakthrough to be achieved, τ', a modified form of the Yoon-Nelson model is obtained:[38]

$$t = \tau' + \frac{\tau'}{k}\ln\left(\frac{C_{out}}{C_{in} - C_{out}}\right) = \tau' + \frac{1}{k'}\ln\left(\frac{C_{out}}{C_{in} - C_{out}}\right) \qquad (18)$$

where τ' is the time at which 50 % breakthrough is achieved (min) and k' is the adsorption kinetic constant (min^{-1}).

3.3.3.2. Results of fitting – Discussion

This model has the advantage that the data related to the gas phase concentrations can be directly fitted to Eq. 18, without the need to determine the quantities of mercury adsorbed on the solid (q). Figure 5 shows the breakthrough curves predicted by the Yoon-Nelson model and compares them to the experimental curves for all the biomass gasification chars. The characteristic parameters of this model, namely the time required to reach 50% of the inlet concentration (τ') and the adsorption kinetic constant, together with the percentage of deviation between the experimental and predicted breakthrough curves and the experimental times required to achieve 50% of the inlet concentration (τ_{exp}') are shown in Table 4.
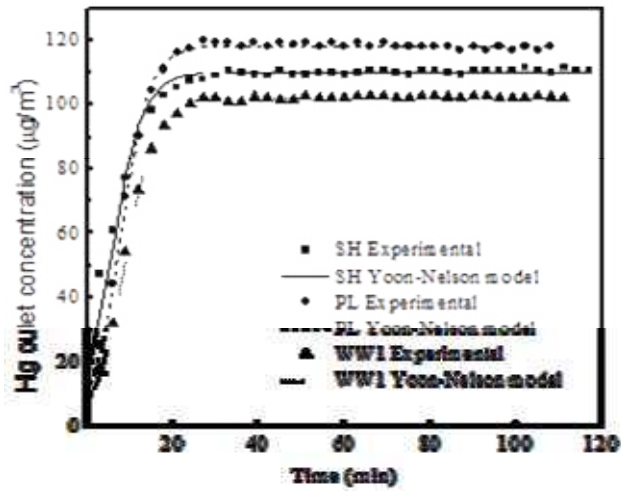
(A)
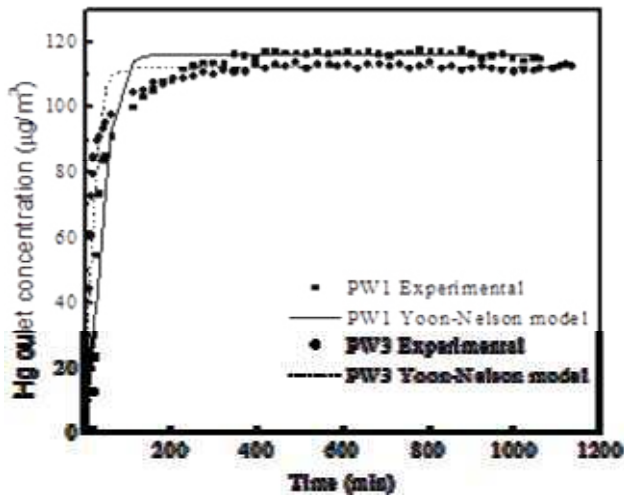
(B)

Figure 5. Experimental and calculated Hg^0 breakthrough curves for the (a) SH, PL and WW1 chars and (b) PW1 and PW3 chars obtained by means of the Yoon-Nelson model.

The global kinetic constants defined by this model take into account the mass transfer balance in the reactor. The values for the PW chars are one order of magnitude smaller than for the chars with a low mercury adsorption capacity. This has also been observed with other models and indicates that in all cases the kinetics of the mercury gas phase uptake is much slower in these chars. The experimental and predicted times needed to reach 50% of the inlet concentration practically coincide for the SH, PL and

WW1 chars, with the PW chars showing the largest discrepancy (approx. 30%) (Table 4). The large differences between τ' and τ_{exp}' in the case of the PW chars are not surprising since there is a strong contribution from adsorption, which is not taken into account in the mass balance in the reactor.

Table 4 - Kinetic data obtained by applying a fixed bed mass balance (Yoon and Nelson model) to the biomass gasification chars.

Sample	R^2	Kinetic constant k' (min^{-1})	Time 50%C_{in} τ'(min^{-1})	Time 50%C_{in} τ'_{exp}(min^{-1})	Deviation (DEV%)
SH	0.967	0.275	5.77	4.72	3.53
PL	0.995	0.306	7.84	7.71	1.64
WW1	0.996	0.291	8.80	9.02	1.45
PW1	0.898	0.0540	36.8	27.7	5.00
PW3	0.857	0.0823	14.5	11.3	3.65

If the percentages of deviation of all the kinetic models are compared, the Yoon-Nelson model is by far the best model for describing mercury adsorption in the chars of low capacity (SH, PL and WW1). As can be seen in Table 4 the percentage of deviation ranges from 1.5 to 3.5% for these samples. This good fitting is confirmed by the clear overlapping of the predicted and experimental breakthrough curves throughout the experiments, Figure 5(a). Moreover, this model also provides a good prediction for the PW chars, since in this case the errors are lower than 5% (Table 4). As can be seen in Figure 5(b), the deviations between the experimental and the predicted breakthrough curves are of great importance at the beginning of the process, at times below 200 minutes. These are reflected in the smaller values of R^2 ($R^2 \sim 0.9$) (Table 4).

In general, as the adsorbed quantities are not really high and the small particle sizes give rise to only a small number of diffusion resistance problems, this model provides

an adequate description of mercury uptake kinetics for all the char samples studied in this work.

4. Conclusions

The group of chars obtained from plastic-paper waste showed the best behaviour for retaining elemental mercury due to their: (i) high chlorine content, (ii) large BET area and (iii) large total pore volume, especially large micropore volume where the mechanism of adsorption tends to be that of pore filling rather than one of surface covering and where the potential for interaction between the solid sorbent and the mercury molecules is significantly greater than in the wider pores.

The Yoon-Nelson model provided the best fit for the samples with low mercury retention capacities as a consequence of their smaller microporosity which favours internal pore diffusion and a rapid breakthrough.

All the models provide relatively accurate predictions for the samples with the highest mercury adsorption capacity (PW) since their intense microporous structure retards the internal diffusion process and their increased chlorine content enhances the chemisorption mechanism on their surface. The successful fitting of the models derived from the Langmuir theory together with the high adsorption temperature used in this study enhances the chemisorption mechanism that involves the oxidation of Hg^0 to Hg^{+1} or Hg^{+2} on the surface of the adsorbents.

All of the models examined describe the experimental behaviour of the fixed bed column with a high degree of accuracy. In short, the kinetic approach adopted in this study contributes to a better understanding of the mercury cleaning process and its design.

References

(1) United Nations Environment Programme (UNEP). Global Mercury Assessment 2013: Sources, emissions, releases, and environmental transport, 42 pp, available in http://www.unep.org.

(2) Sudseth, K.; Pacyna, M. J.; Pacyna, G. E.; Munthe, J.; Belhaj, M.; Astrom, S. Economic benefits from decreased mercury emissions: Projections for 2020. *J. Cleaner. Prod.* **2010**, *18*, 386.

(3) Wang, Y.; Duan, Y.; Yang, L.; Zhao, Ch.; Shen, X.; Zhang, M; Zhuo, Y; Chen Ch. Experimental study on mercury transformation and removal in coal fired boiler flue gases. *Fuel Process. Technol.* **2009**, *90*, 643.

(4) Asasian, N.; Kaghazchi, T.; Soleimani, M. Elimination of mercury by adsorption onto activated carbon prepared from the biomass material. *J. Ind. Eng. Chem.* **2012**, *18*, 283.

(5) Skodras, G.; Diamantopoulou, Ir.; Zabaniotou, A.; Stavropoulos, G.; Sakellaropoulos, G. Enhanced mercury adsorption in activated carbon from biomass materials and waste tires. *Fuel Process. Technol.* **2007**, *88*, 749.

(6) Zengqiang, T.; Jianrong, Q.; Hancai, Z.; Hao, L.; Jun, X. Removal of elemental mercury by bamboo charcoal impregnated with H_2O_2. *Fuel* **2011**, *90*, 1471.

(7) Abad-Valle, P.; López-Antón, M. A.; Díaz-Somoano, M.; Martínez-Tarazona, M. R. The role of unburned carbon concentrates from fly ashes in the oxidation and retention of mercury. *Chem. Eng. J.* **2011**, *174*, 86.

(8) Lopez-Anton, M. A.; Perry, R.; Abad-Valle, P.; Diaz-Somoano, M.; Martinez-Tarazona, M. R.; Maroto-Valer, M. M. Speciation of mercury in fly ashes by temperature programmed desorption. *Fuel Process. Technol.* **2011**, *92*, 707.

(9) Fuente-Cuesta, A.; Diaz-Somoano, M.; Lopez-Anton, M. A.; Cieplik, M.; Fierro, J L. G.; Martinez-Tarazona, M. R. Biomass gasification chars for mercury capture from a simulated flue gas of coal combustion. *J. Environ. Manage.* **2012**, *98*, 23.

(10) Fuente-Cuesta, A.; Lopez-Anton, M. A.; Diaz-Somoano, M. Martinez-Tarazona, M. R. Retention of mercury by low-cost sorbents: Influence of flue gas composition and fly as occurrence. *Chem. Eng. J.* **2012**, *213*, 16.

(11) Liu, W.; Yin, P.; Liu, X.; Dong, X.; Zhang, J.; Xu, Q. Thermodynamics, Kinetics, and isotherms studies for gold(III) adsorption using silica functionalized by diethylenetriaminemethylenephosphonic acid. *Chem. Eng. Res. Des.* **2013**, *91*, 2748.

(12) Shafeeyan, M. S.; Wan Daud, W. M. A.; Shamiri, A. A review of mathematical modeling of fixed-bed columns for carbon dioxide adsorption. *Chem. Eng. Res. Des.* **2014**, *92*, 961.

(13) Camargo, C. L. M.; De Resende, N. S.; De Oliveira, A. G.; Salim, V. M. M.; Tavares, F. W. Investigation of adsorption-enhanced reaction process of mercury removal from simulated natural gas by mathematical modeling. *Fuel* **2014**, *129*, 129.

(14) Chung, T. S.; Kim II, K.; Yun, R. Y. Adsorption of elemental mercury vapour by impregnated activated carbon from a commercial respirator cartridge. *Power Technol.* **2009**, *192*, 47.

(15) Flora, V. R. Y.; Hargis, A. R.; O'Dowd, J. W.; Pennline, W. H.; Vidic, D. R. Modelling sorbent injection for mercury control in bag house filters: I-mode development and sensitivity analysis. *J. Air Waste Manage.* **2003**, *53*, 478.

(16) Zhao, B.; Zhang, Zh.; Jin, J.; Pan, Wei-Ping. Simulation of mercury capture by sorbent injection using a simplified model. *J. Hazard. Mater*. **2009**, *170*, 1179.

(17) Mohan, D.; Gupta, K. V.; Srivastava, K. S.; Chander, S. Kinetics of mercury adsorption from wastewater using activated carbon derived from fertilizer waste. *Colloid surface A* **2001**, *177*, 169.

(18) Wajima, T.; Sugawara, K. Adsorption behaviours of mercury from aqueous solution using sulphur-impregnated adsorbents developed from coal. *Fuel Process. Technol.* **2011**, *92*, 1322.

(19) Ho, S. Y. Citation review of Lagergren kinetic rate equation on adsorption reactions. *Scientometrics* **2004**, *59*, 171.

(20) Ho, S. Y.; McKey, GHo. Pseudo-second order model for sorption processes. *Process. Biochem.* **1999**, *34*, 451.

(21) Skodras, G.; Diamantopoulou, Ir.; Pantoleontos, G.; Sakellaropoulos, G. P. Kinetic studies of elemental mercury adsorption in activated carbon fixed bed reactor. *J. Hazard. Mater.* **2008**, *158*, 1.

(22) Jagiello, J.; Thommes, M. Comparison of DFT characterization methods based on N_2, Ar, CO_2, and H_2 adsorption applied to carbons with various pore size distributions. *Carbon* **2004**, *42*, 1227.

(23) Silvestre-Albero, J.; Silvestre-Albero, A.; Rodríguez-Reinoso, F.; Thommes, M. Physical characterization of activated carbons with narrow microporosity by nitrogen (77.4K), carbon dioxide (273K) and argon (87.3K) adsorption in combination with immersion calorimetry. *Carbon* **2011**, *50*, 3128.

(24) Liu, J.; Cheney, A. M.; Wu, F.; Li, M. Effects of chemical functional groups on elemental mercury adsorption on carbonaceous surfaces. *J. Hazard. Mater.* **2011**, *186*, 108.

(25) Azizian, S. Kinetic models of sorption: a theoretical analysis. *J. Colloid Interface Sci.* **2004**, *276*, 47.

(26) Ho, S. Y.; McKay, G. A comparison of chemisorption kinetic models applied to pollutant removal on various sorbents. Process Saf. Environ. **1998**, *76*, 332.

(27) Hill, CJr. An introduction to chemical engineering kinetics and reactor design, John Wiley & Sons, New York, pp. 176-177, 1977.

(28) Ho, S. Y. Review of second-order models for adsorption systems. *J. Hazard. Mater.* **2006**, *136*, 681.

(29) Reddad, Z.; Gerente, C.; Andres, Y.; Cloirec, P. Adsorption of several metal ions onto a low-cost biosorbent: Kinetic and Equilibrium Studies. *Environ. Sci. Technol.* **2002**, *36*, 2067.

(30) Diamantopoulou, Ir. Mercury removal from flue gases with adsorption on activated carbons. Aristotle University of Thessaloniki, Greece, PhD thesis, 2008.

(31) Skodras, G.; Grammelis, P.; Basinas, P.; Kaldis, S.; Kakaras, E.; Sakellaropoulos, G. P. A kinetic study on the devolatilisation of animal derived byproducts. *Fuel Process. Technol.* **2007**, *88*, 787.

(32) Ruthven, M. D. Principles of adsorption and adsorption processes, John Wiley & Sons Publications, New York, pp. 168-169, 1984.

(33) Crank, J. *The mathematics of diffusion*; Clarendon Press. Oxford, p. 47 and p. 91, 1975.

(34) Pantoleontos, G.; Basinas, P.; Skodras, G.; Grammelis, P.; Pintér, J. D.; Topis, S.; Sakellaropoulos, G. P. A global optimization study on the devolatilisation kinetics of coal, biomass and waste fuels. *Fuel Process. Technol.* **2009**, *90*, 762.

(35) Wang, S.; Li, H. Kinetic modelling and mechanism of dye adsorption on unburned carbon. *Dyes Pigments* **2007**, *72*, 308.

(36) Wheeler, A.; Robell, A. J. Performance of fixed bed catalytic reactors with poison in the feed. *J. Catal.* **1969**, *13*, 299.

(37) Quintelas, B.; Fernandez, C.; Castro, J.; Figuereido, H.; Tavares, T. Biosorption of Cr(IV) by a Bacillus Coagullans biofilm supported on granular activated carbon (GAC). *Chem. Eng. J.* **2008**, *136*, 195.

(38) Mastral, M. A.; Garcia, T.; Murillo, R.; Callen, S. M.; Lopez, M. J.; Navarro, V. M. Effects of CO2 on the Phenanthrene Adsorption Capacity of Carbonaceous Materials. *Energ. Fuel* **2002**, *16*, 510.

(39) Wood, G. O.; Stampfer, F. J. Adsorption rate coefficients for gases and vapors on activated carbons. *Carbon* **1993**, *31*, 195.

Figure captions

Figure 1. Schematic diagram of the lab-scale experimental device for mercury retention.

Figure 2. Hg^0 breakthrough curves (a) Sunflower husks, poultry litter and waste wood chars (b) plastic-paper chars.

Figure 3. Experimental and calculated Hg^0 breakthrough curves for the (a) SH and (b) PW1 chars obtained by means of pseudo-first and pseudo-second order models.

Figure 4. Experimental and calculated Hg^0 breakthrough curves for the (a) SH and (b) PW1 chars obtained by means of the Diffusion model.

Figure 5. Experimental and calculated Hg^0 breakthrough curves for the (a) SH, PL and WW1 chars and (b) PW1 and PW3 chars obtained by means of the Yoon-Nelson model.